Intracellular FUS protein accumulation leads to cytoskeletal, organelle and cellular homeostasis perturbations

Chyi Wei Chung[a], Alexandra J. Zhou[b,c], Ioanna Mela[a], Amberley D. Stephens[a], Akinori Miyashita[d,1], Peter H. St George-Hyslop[d,e,f], Clemens F. Kaminski[a], Tuomas P. J. Knowles[b,c], Gabriele S. Kaminski Schierle[a*]

[a] Department of Chemical Engineering and Biotechnology, University of Cambridge, CB3 0AS, United Kingdom.
[b] Centre for Misfolding Diseases, Yusuf Hamied Department of Chemistry, University of Cambridge, CB2 1EW, United Kingdom.
[c] Cavendish Laboratory, Department of Physics, University of Cambridge, CB3 0HE, United Kingdom.
[d] Department of Medicine (Neurology), Temerty Faculty of Medicine, University of Toronto, and University Health Network, 60 Leonard Avenue, Toronto, ON M5T 0S8, Canada.
[e] Cambridge Institute for Medical Research and Department of Clinical Neurosciences, School of Clinical Medicine, Addenbrookes Biomedical Campus, University of Cambridge, CB2 0XY, United Kingdom.
[f] Taub Institute for Research on Alzheimer's Disease and the Aging Brain, Department of Neurology, Columbia University Irvine Medical Center, 630 West 168th Street, New York, NY, USA 10032.

[1] Present address: Department of Molecular Genetics, Brain Research Institute, Niigata University, Niigata, Japan.

*Corresponding author: gsk20@cam.ac.uk

Summary

The molecular mechanisms that connect the formation of aberrant cytoplasmic FUS condensates to biological malfunction are incompletely understood. Here, we develop an approach to determine the intracellular FUS viscosity in live mammalian cells and find that ALS-related mutant P525L-FUS forms the most viscous condensates and has impaired cytoskeletal mechanoproperties and increased euchromatin formation. We further show that some of the main cellular organelles, e.g., actin/tubulin, lysosomes, mitochondria, the endoplasmic reticulum, are significantly functionally/structurally impaired in the presence of FUS. These may be related to defects in the tubulin network, as the latter facilitates transport, formation, fusion and fission of organelles. We observe significant increases in lysosomal biogenesis, size and pH; moreover, intracellular FUS accumulation significantly promotes cytoplasmic-to-nuclear translocation of TFEB, i.e., the master gene for inducing autophagy. However, despite these, increased autophagy needed for protein aggregate clearance is not observed to occur. Our study reveals that the formation of highly viscous FUS condensates significantly impacts cytoskeletal/organelle function and cellular homeostasis, which are closely associated with cell ageing. This raises the intriguing question as to whether mutant FUS activates similar cell processes as those during cellular senescence.

Keywords: fused-in sarcoma, amyotrophic lateral sclerosis, frontotemporal dementia, lysosomal de-acidification, TFEB, cytoskeletal defects, organelle dysfunction, autophagy-lysosomal pathway.

Introduction

The aberrant condensation of fused-in sarcoma (FUS) is a hallmark of both amyotrophic lateral sclerosis (ALS) and frontotemporal dementia (FTD). Under physiological conditions, FUS undergoes liquid-liquid phase separation (LLPS) and exists in a liquid and/or a dense condensate state predominantly within cell nuclei. Prominent cytoplasmic mislocalisation and the formation of more viscous, and in many cases, gelled condensates or even fibrillar aggregates, are observed upon missense and truncation mutations. Many, but not all of these ALS-associated mutations occur within the FUS nuclear localisation signal (NLS) (Bosco et al., 2010; Conte et al., 2012; Waibel et al., 2010). Pathological phase separation and the formation of gelled condensates have also been linked to arginine hypomethylation of FUS, as commonly observed in cases of sporadic FTD, which leads to disruptions in cytoplasmic ribonucleoprotein (RNP) granule function (e.g., stress granules (SGs) and neuronal transport granules) (Hofweber et al., 2018; Murakami et al., 2015; Qamar et al., 2018).

Whilst much attention has been given to the pathological role of FUS in the formation of cytoplasmic SGs, an understanding of how FUS condensation leads to disturbances in cellular homeostasis and function would be invaluable. This knowledge could also yield avenues for therapeutic intervention in diseases associated with the aberrant assembly of these proteins, such as FUS-associated ALS (fALS-FUS) and frontotemporal lobar degeneration (FTLD-FUS).

A potentially powerful clue to the latter may come from a detailed analysis of different fALS-FUS and FTLD-FUS models. We thus first established different FUS expressing cell lines and stress models in HEK293T cells before comparing the changes in intracellular FUS viscosity of the various FUS models. Combining single particle tracking (SPT-) and fluorescence lifetime imaging microscopy (FLIM), we develop a method to quantify intracellular FUS viscosity without the need for an external sensor/tracer, and that is higher-throughput than conventional fluorescence recovery after photobleaching (FRAP). To understand how FUS condensation leads to disturbances in cellular homeostasis, we then focused our analysis on the role of FUS in the nucleus and the cytoplasm,

64 including its effect on the cytoskeleton and on organelle positioning and function. We show that P525L-
65 FUS cells form the most viscous condensates, which affect the level of euchromatin formation,
66 cytoskeletal proteins and organelle positioning and function, including lysosomes, mitochondria and
67 the endoplasmic reticulum (ER). We show that the latter is linked to the observed lysosomal de-
68 acidification, which acts as a trigger for the nuclear to cytoplasmic translocation of transcription factor
69 EB (TFEB), i.e., the master modulator of autophagic genes. Instead of the expected upregulation of
70 macroautophagy (henceforth referred to as autophagy), however, autophagy is blocked at an early
71 stage, which promotes cellular malfunction and disease progression (Aman et al., 2021; Martini-Stoica
72 et al., 2016).

73

74

Results

Fluorescence lifetime imaging and single particle tracking form a tool to measure FUS condensate viscosity in live cells

Studying phase separation in live cells, and thus characterising intracellular FUS viscosity is challenging (Kuimova, 2012). We have previously shown, however, that protein phase separation and aggregation can be measured *in vitro* and in live cells using FLIM (Chen et al., 2017; Esbjörner et al., 2014). We thus first investigated whether SPT, which permits exact viscosity measurements *in vitro*, can be correlated with FLIM. We generated LLPS condensates by mixing equal amounts of recombinant GFP- and unlabelled WT-FUS protein. We then added the protein mixture into a solution containing 10% polyethylene glycol 35 (PEG-35) and 150 mM potassium chloride (KCl) to mimic the molecular crowding and ionic environments of the nuclear and cytoplasmic intracellular compartments. As we were interested in aggregation kinetics and changes in the micro-rheology of FUS with time, we performed ageing experiments involving SPT and FLIM over time, giving us a means to quantify both parameters of interest (**Figure 1A**). To probe the viscosity within FUS condensates, we introduced 40 nm fluorescent nanoparticles into the condensate mixture and tracked their trajectories. Because fluctuations seen in tracked nanoparticle trajectories are predominantly due to Brownian motion (Crocker and Grier, 1996); hence, we were able to calculate intra-condensate FUS viscosity from their mean square displacement (MSD) profiles. Between the 0 to 1h time points, FUS in the condensates becomes more viscous, with viscosity values increasing from 0.11±0.01 Pas to 0.44±0.08 Pas (**Figure 1B**, blue points). We observe a correlation between FLIM and SPT measurements (**Figure 1B**). During the same time period during which increased viscosity is observed, the GFP-tagged FUS molecules in the condensates cluster more closely, as indicated from the decrease in their fluorescence lifetimes from 2.23±0.01 ns to 2.08±0.01 ns (**Figure 1B**, red points; **Figure 1C**, Condensates). These values are in turn lower than that of dispersed WT-FUS before LLPS at 2.53 ns (**Figure 1B,** green point; **Figure 1C**, dispersed), which has a viscosity of 0.004 Pas from SPT measurements. To induce the fibrillation of FUS, we removed PEG-35 from the

100 condensate mixture described above to yield solid fibrils with a fluorescence lifetime in the range of
101 2.01±0.01 ns (**Figure 1B**, magenta point; **Figure 1C**, Fibrils). As the fluorescence lifetime of GFP is
102 independent of the viscosity of its surrounding environment (Davidson et al., 2020), we note that FLIM
103 and SPT yield independent and complementary parameters indicative of the level of FUS compaction
104 and viscosity, respectively. Our data further show that beyond an hour, there are no further significant
105 changes in either fluorescence lifetime or viscosity.

106 To observe both physiological and aberrant condensate formation of FUS in a cell model, we
107 created HEK293T cells expressing GFP-labelled FUS (**Figure S1A**). To ensure that our observations were
108 not due to the accumulation of GFP, we included cells expressing a GFP only construct (i.e., Control) in
109 our experiments. We studied WT-FUS, and two ALS-related mutants, (i.e., P525L and R495X with a point
110 site mutation at and truncation of the NLS, respectively), thereby leading to cytoplasmic mislocalisation
111 of FUS(Gonzalez et al., 2021). Pathological phase separation of FUS is also promoted upon
112 hypomethylation of its arginine-rich domain, yielding irreversible FUS hydrogels that are prevalent in
113 FUS-related forms of sporadic FTD (Hofweber et al., 2018; Murakami et al., 2015). In order to induce
114 FUS hypomethylation, we treated the cells with adenosine periodate oxidase (AdOx), an arginine
115 methyltransferase inhibitor, which modulates the methylation state of the RNA-binding, arginine-rich
116 domain of FUS (Fujii et al., 2016; Qamar et al., 2018). This promotes gelation and results in the
117 formation of clusters of hypomethylated (HYPO) intranuclear aggregates (**Figure S1B**). P525L-FUS cells
118 lose cytoplasmic mislocalisation, whereas R495X-FUS cells (which have a truncated NLS) still retain
119 cytoplasmic condensates after AdOx treatment. Furthermore, we induced the formation of SGs using
120 sodium arsenite ($NaAsO_2$) (**Figure S1C**). Existing as membraneless LLPS structures of cytoplasmic RNPs,
121 SGs are transient structures of translationally stalled mRNA complexes and proteins (Sama et al., 2013).
122 However, it has been suggested that in neurodegeneration models, they become persistent and are
123 the site of aberrant aggregation (Wolozin and Ivanov, 2019). We validated the formation of SGs in our
124 cell models by immunostaining of Ras-GTPase-activating protein binding protein (G3BP), a protein
125 marker for the assembly and dynamics of SGs (**Figure S2**) (Yang et al., 2020). Agreeing with previous

126 reports (Baron et al., 2013; Bosco et al., 2010), we observe colocalisation of FUS and G3BP only in the
127 case of mutant variants of FUS (**Figure S2B**), despite the formation of SGs in all cell models.

128

129 ALS-associated FUS mutants form the most viscous aggregates in live cells

130 Using FLIM, we could quantify the aggregation propensity and extent of FUS in our cell models (**Figure**
131 **1D&E**). We observe that the NLS-mutants have more aggregated FUS (cell-averaged values of 2.48±0.12
132 ns and 2.49±0.12 ns for P525L- and R495X-FUS, respectively), in comparison to nuclear-localised WT-
133 FUS (2.62±0.07 ns) with fluorescence lifetimes that do not differ significantly from control cells at
134 2.64±0.06 ns. As FUS in SGs and hypomethylated intranuclear aggregates have higher fluorescence
135 intensities than other compartments of the cell (**Figure S1B&C**), we could segment them by setting a
136 fluorescence intensity threshold (**Figure 1D,** AdOx & $NaAsO_2$). In comparison to R495X-, P525L-FUS has
137 a lower fluorescence lifetime than hypomethylated intranuclear aggregates (1.78±0.05 ns *cf.* 2.01±0.04
138 ns in R495X) and SGs (2.35±0.06 ns *cf.* 2.46±0.02 ns in R495X). To calculate the intracellular viscosity of
139 FUS, we created a fluorescence lifetime to viscosity calibration based on the *in vitro* FUS condensate
140 system (**Figure S3A**), noting that GFP fluorescence lifetimes of recombinant FUS and the HEK293T FUS
141 models fall within the same range of 1.6—2.6 ns (**Figure 1E**). Hence, we perform linear fitting (**Figure**
142 **S3A**, black line) on SPT-FLIM data of the *in vitro* protein condensate system (**Figure S3A**, grey circles),
143 to map fluorescence lifetime values of FUS imaged in live HEK293T cells to their corresponding viscosity
144 values (**Figure 1E**, secondary axis). We note that before both AdOx and $NaAsO_2$ treatment, the two NLS
145 mutants of FUS are more viscous at ~0.10 Pas than WT-FUS at 0.05 Pas. Moreover, we estimate that
146 hypomethylated aggregates differ in their viscosity to SGs by a factor of 5—10, i.e., 0.69±0.05 (AdOx –
147 P525L) to 0.14±0.06 Pas ($NaAsO_2$ – P525L) and 0.47±0.04 (AdOx – R495X) to 0.04±0.02 Pas ($NaAsO_2$ –
148 R495X.

149 We observe a similar trend upon calculating the diffusion coefficient of these FUS macro-
150 assemblies inside cells (**Figure S3B**). For the latter, we extracted MSD profiles of the FUS macro-
151 assemblies' trajectories over time, which we imaged in a similar manner to SPT measurements for the
152 *in vitro* condensates. For both, AdOx and $NaAsO_2$ treatments, P525L-FUS cells yield HYPO nuclear
153 aggregates and SGs of lowest mobility, with respective diffusion coefficients of 0.036±0.004 nm^2 s^{-1}
154 (compared to 0.044±0.004 nm^2 s^{-1} in WT-FUS cells) and 0.011±0.002 nm^2 s^{-1} (compared to 0.025±0.001
155 nm^2 s^{-1} in R495X-FUS cells). As aforementioned, R495X-FUS is the only model that retains the
156 cytoplasmic distribution of FUS upon AdOx treatment due to its truncated NLS (**Figure S1B**). We observe
157 that the hypomethylated aggregates it forms are the most mobile with a diffusion coefficient
158 0.076±0.007 nm^2 s^{-1} (i.e., two-fold that of P525L- and WT-FUS). Hence, using both, our fluorescence
159 lifetime to viscosity calibration as well as diffusion coefficient measurements, we show that there are
160 differences in the way different FUS variants interact with their nuclear and cytoplasmic environment,
161 which affect their aggregation propensity.

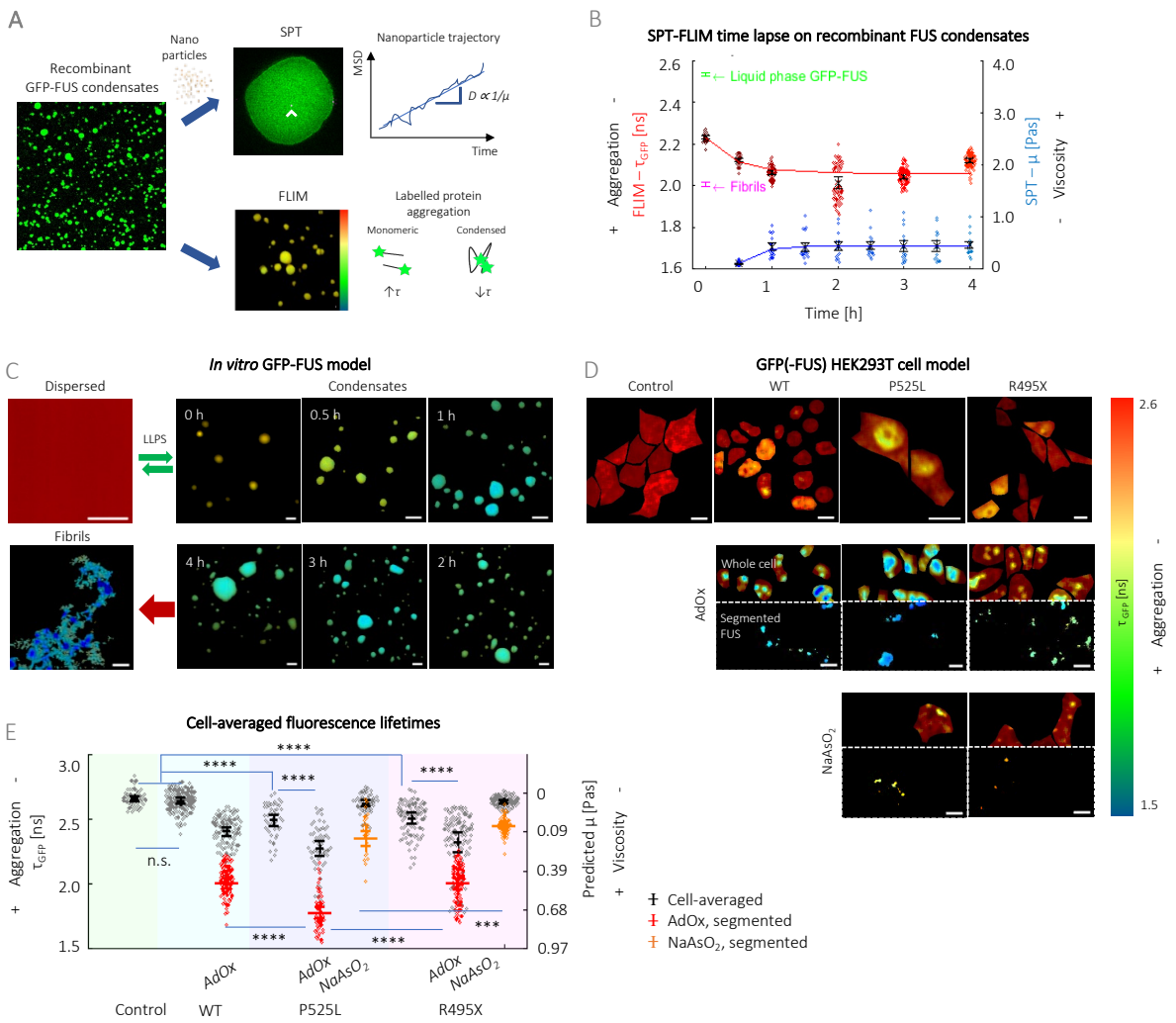

Figure 1: Fluorescence lifetime to viscosity calibration reveals that ALS-associated P525L-FUS forms the most viscous condensates. (A) FLIM and SPT measurements were performed on *in vitro* FUS condensates, giving a measure of condensation state and viscosity, respectively. For SPT, 40 nm nanoparticles (denoted by white arrowhead) were mixed into the condensates and the mean square displacement (MSD) profiles of their trajectory were analysed. (B) Combined SPT-FLIM data show that there is a trend between GFP fluorescence lifetimes (τ_{GFP}, FLIM in red) and viscosity (μ, SPT in blue), where more aged FUS condensates are also more viscous. Values plateau ~1 hour and show no further change upon subsequent ageing. (C) Fluorescence lifetime maps for liquid-to-solid transition of recombinant FUS. A decrease in τ_{GFP} is used to quantify increasing condensation as dispersed FUS undergoes LLPS to form condensates, which are aged over a 4-hour period. Upon irreversible solid transition (i.e., formation of fibrils), fluorescence lifetime values are at the lowest values at 2.01±0.01 ns. Scale bars, 10 μm. (D) Fluorescence lifetime maps for FUS in the GFP HEK293T model, which show that fluorescence lifetimes fall in the same 1.5—2.6 ns range as the *in vitro* system in (C). The formation of hypomethylated (HYPO) intranuclear aggregates (first row, AdOx) and SGs (second row, $NaAsO_2$) were induced by the addition of different stressors. These macro-assemblies can

175 be easily segmented by fluorescence intensity thresholding (Segmented FUS). Scale bars, 10 µm. (E) Cell averaged-
176 fluorescence lifetimes values (black) alongside viscosity predicted from correlative FLIM-SPT calibration on in vitro
177 condensates (B). ALS-related FUS mutant cells have lower τ_{GFP} (i.e., are at a more condensed state) in comparison to WT-FUS
178 and control cells. Fluorescence lifetimes of segmented hypomethylated nuclear aggregates (AdOx, red) and SGs ($NaAsO_2$,
179 orange) are also given, with P525L- forming more viscous macroassemblies compared to R495X-FUS. *In vitro* and HEK293T
180 FUS cell measurements were based on 3 individual protein preparations and 3 biological repeats respectively. One-way ANOVA
181 test (with Holm-Sidak's multiple comparison), where n.s. is not significant, *** $p<0.001$ and **** $p<0.0001$.

182

183 P525L-FUS mutant impairs cellular mechanoproperties and enhances euchromatin 184 formation

185 We have thus far established that there are differences in the condensation states of FUS, with mutant
186 P525L- and R495X-FUS being in a more condensed state than WT-FUS, even if the latter has been
187 exposed to stressors such as AdOx and $NaAsO_2$. It has been suggested that loss of FUS functionality and
188 its cytoplasmic mislocalisation can cause loss or gain of function defects by affecting essential
189 cytoskeletal proteins (Theunissen et al., 2021). To further characterise the latter in our HEK293T cell
190 models, we visualise filamentous (f-)actin and microtubules (i.e., the 2 main proteins of the
191 cytoskeleton) using far-red fluorogenic Silicon Rhodamine (SiR) dyes (Lukinavičius et al., 2014) (**Figure**
192 **2**). As the SiR-dyes are of high specificity and only become fluorescent upon binding, their fluorescence
193 intensity can be used as to measure f-actin and microtubule polymerisation levels. Our data reveal that
194 only P525L- and not R495X-FUS has a significant impact on the cytoskeleton, as shown by reduction of
195 f-actin, as shown by a loss in SiR-Actin intensity. A similar effect on SiR-Actin intensity can only be
196 induced by stressors, such as AdOx and $NaAsO_2$, which cause hypomethylation or SG formation,
197 respectively (**Figure 2A&B**). However, in the case of P525L-FUS, the above stressors do not cause a
198 further defect on the cytoskeleton as P525L-FUS alone does. We next used SiR-Tubulin and performed
199 similar experiments as described above to see whether FUS condensates would also affect the
200 microtubule protein, tubulin. It is observed that P525L-FUS, followed by R495X-FUS, cells have the
201 lowest SiR-Tubulin intensity levels prior to drug treatments. Interestingly though, AdOx treatment,

which promotes nuclear translocation of FUS and the formation of hypomethylated clusters, reduces the burden on microtubules mainly present in the cytoplasmic region, the effect being strongest in P525L-FUS cells, where the largest drop in SiR-Tubulin intensity has occurred prior to the addition of AdOx (**Figure 2C&D**). The opposite effect is seen when cytoplasmic SGs are formed using $NaAsO_2$, which results in significantly reduced SiR-Tubulin intensities in all models. Additionally, we quantified the amounts of f-actin and β-tubulin (a sub-unit of microtubules) in the cell samples based on a Western Blot (**Figure S4**), and we find they do not differ significantly between FUS variants. Hence, this may indicate that depolymerisation of actin and microtubules has occurred, instead of lower concentrations of either being expressed.

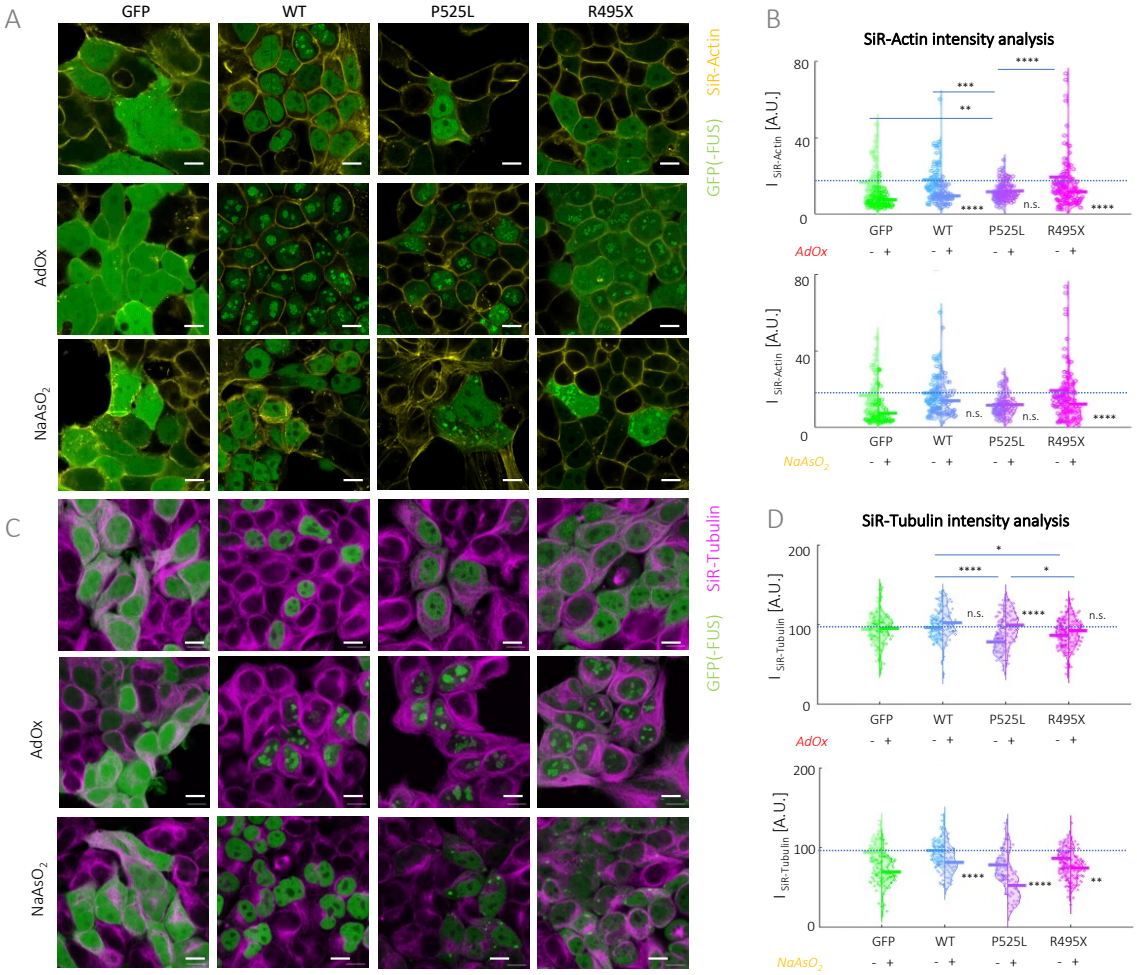

Figure 2: ALS-associated P525L-FUS has lowered levels of important cytoskeletal proteins based on SiR-dye staining. (A) Fluorescence intensity composite images for GFP(-FUS) (green) and SiR-Actin (yellow). Scale bars, 10 µm. (B) Cell-averaged fluorescence intensity

214 quantification for SiR-Actin ($I_{SiR\text{-}Actin}$). f-actin levels in P525L-FUS cells are low even without the addition of any stressors. AdOx has a greater
215 effect in comparison to $NaAsO_2$ on reducing f-actin levels. (C) Fluorescence intensity composite images for GFP(-FUS) (green) and SiR-Tubulin
216 (magenta). Scale bars, 10 µm. (D) Cell-averaged fluorescence intensity quantification for SiR-Tubulin ($I_{SiR\text{-}Tubulin}$). Tubulin levels in P525L- and
217 R495X-FUS cells are impacted even without the addition of any stressors. The formation of HYPO aggregates improves microtubule levels, in
218 contrast to SGs which impair microtubules. HEK293T measurements were based on 3 biological repeats. One-way ANOVA test (with Holm-
219 Sidak's multiple comparison), where * for $p<0.05$, ** $p<0.01$, *** $p<0.001$, **** $p<0.0001$.

220 To confirm that FUS condensates indeed affect cellular mechanoproperties by interfering with
221 the two most important cytoskeletal proteins, actin and tubulin, we perform force-displacement (FD)-
222 atomic force microscopy (AFM) measurements on the cytoplasmic regions of live cells (**Figure S5**). In
223 comparison to WT-FUS cells, we have seen that mutant P525L-FUS cells display the lowest levels of
224 polymerisation for both cytoskeletal proteins investigated; moreover, R495X-FUS cells have lower levels
225 of SiR-Tubulin detected (**Figure 2**). Corroborating this, we find that P525L-FUS cells have the softest
226 cytoplasm with an average apparent Young's modulus (E_{App}) of 12.3±2.2 kPa, followed by R495X at
227 13.7±4.0 kPa, in comparison to WT-FUS at 25.5±2.2 kPa (**Figure S5A**); these measurements correspond
228 to intensity quantifications of SiR-dyes (**Figure 2**). Hence, we believe that the softening we observe is
229 due to destabilisation of the cytoskeleton i.e., a decrease in E_{App} corresponds to lower intensities of the
230 SiR-dyes (**Figure S5B**). It is interesting to note that the expression of a cytoplasmic protein, such as GFP
231 in the control cells, also has an effect on the cell mechanoproperties as measured by FD-AFM. However,
232 in contrast to FUS cells, which mainly leads to accumulation in the nucleus for WT-FUS and some
233 cytoplasmic condensates in P525L- and R495X-FUS cells, no effect on the cytoskeletal proteins is
234 observed in GFP control cells.

235 We have shown above that AdOx treatment has a significant effect on FUS condensate
236 formation, but AdOx is also known as a drug that reduces DNA methylation. We therefore investigated
237 the effect FUS condensates might have on the level of euchromatin formation, which is strongly
238 increased by hypomethylation. We have recently shown that the dye SiR-DNA (or SiR-Hoechst) can be
239 used to determine the level of eu/heterochromatin formation in live cells (Hockings et al., 2020; Novo
240 et al., 2022). As SiR-DNA intercalates with DNA structures, its fluorescence lifetime is significantly

241 affected by the level of chromatin condensation. Since euchromatin formation is associated with
242 significant DNA decondensation, an increase in the fluorescence lifetime of SiR-DNA can be associated
243 with an increase in euchromatin formation (Hockings et al., 2020; Novo et al., 2022). We observe that
244 both FUS mutant cells contain more euchromatin (i.e., more decondensed DNA), with P525L-FUS cells
245 (3.44±0.03 ns) experiencing a greater extent of DNA decondensation than R495X-FUS cells (3.43±0.04
246 ns) and in comparison to the GFP control (3.40±0.03 ns) and WT-FUS cells (3.41±0.03 ns) (**Figure 3C&D**).
247 To further control our results, we applied two different drugs known to hinder DNA compaction, i.e.,
248 AdOx (due its effect on DNA hypomethylation (Schwerk and Schulze-Osthoff, 2005)) and Trichostatin A
249 (TSA, which induces histone diacetylase (HDAC) inhibition (Moreira et al., 2003; Vigushin et al., 2001))
250 to control cells, which also raised the fluorescence lifetime of SiR-DNA to 3.44±0.04 and 3.43±0.03 ns,
251 respectively. It is interesting to note that the effect aberrant FUS condensates has on euchromatin
252 formation is as severe as the one induced by drugs, such as AdOx and TSA. Taken together, cytoskeletal
253 defects as well as changes in euchromatin state are most prevalent in mutant variants of FUS, especially
254 P525L-FUS.

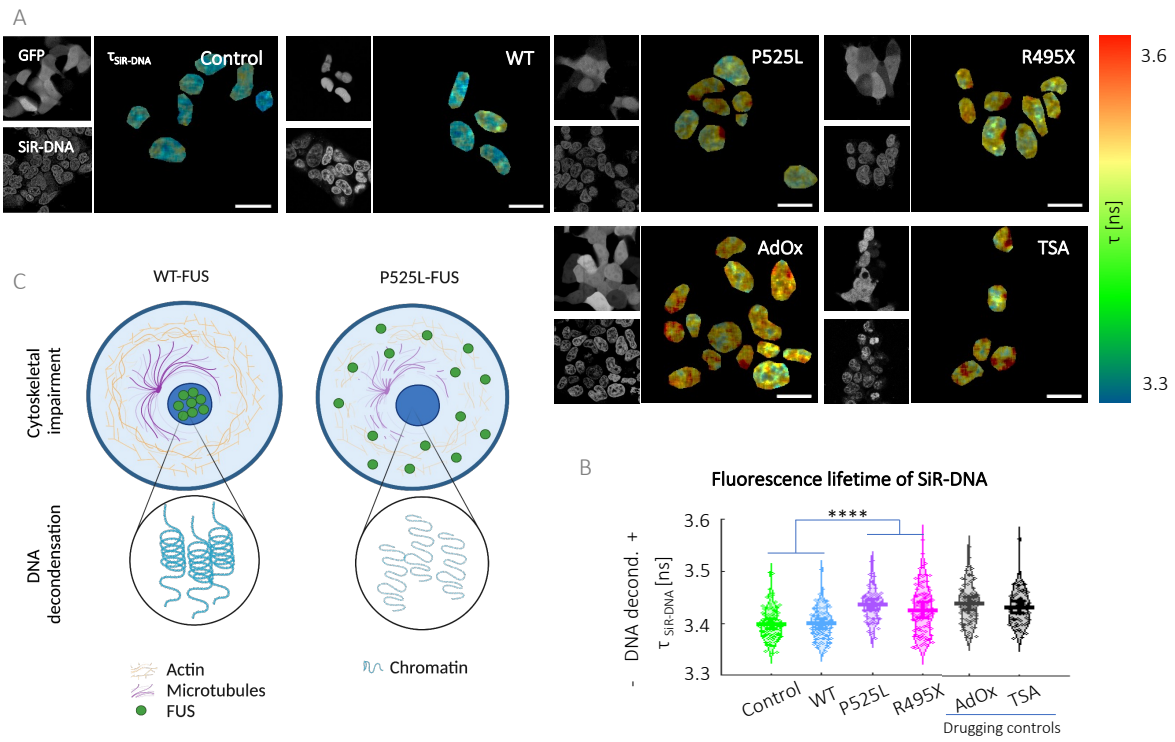

Figure 3: ALS-related FUS mutants lead to an increase in euchromatin formation. (A) Fluorescence lifetime of SiR-DNA is used as a measure of DNA decondensation, which is related to heterochromatin formation. Mutant FUS cells exhibit lower level of heterochromatin formation (i.e., higher $\tau_{SiR\text{-}DNA}$). GFP control cells treated with AdOx and TSA which cause DNA hypomethylation and HDAC inhibition, were included. (B) Fluorescence lifetime maps. Scale bars, 10 µm. (C) Cartoon illustration of impaired mechanoproperties of P525L-FUS cells due to weakened cytoskeleton and DNA damage in comparison to WT-FUS cells. Created on Biorender.com. HEK293T measurements were based on 3 biological repeats. One-way ANOVA test (with Holm-Sidak's multiple comparison), where * for $p<0.05$, ** $p<0.01$, *** $p<0.001$, **** $p<0.0001$.

Aberrant FUS aggregation impacts normal organelle function

The above studies have shown that mutant FUS has a significant effect on the cytoskeleton, which, in particular for tubulin. We thus investigated whether this effect on the microtubules might interfere with organelles, such as lysosomes, mitochondria, and ER, as the microtubules are important for the positioning, formation, fission, and fusion of the latter (Mattenberger et al., 2003; Pu et al., 2016). We applied super-resolution 2-colour structured illumination microscopy (SIM) with a resolution of 100 nm (i.e., below the diffraction limit) (Young et al., 2016) in COS7 cells, which have a flat morphology ideal

271 for SIM, as the technique is sensitive to out-of-focus glare associated with thicker samples (Ma et al.,
272 2021). We show that clustering of lysosomes and mitochondria at the perinuclear area of cells is greater
273 in P525L-, compared to WT-FUS and control cells (**Figure S6**). We have recently found that lysosomes
274 are responsible for the maintenance of the tubular ER network in the periphery of cells (Lu et al., 2022,
275 2020). Thus, clustering of lysosomes in the perinuclear area may significantly impair the tubular ER
276 network in the cell periphery. Hence, to investigate if a collapse in the tubular ER structure also follows
277 upon intracellular FUS accumulation, we co-expressed an ER marker, mEmerald-sec61β (Nixon-Abell et
278 al., 2016) in mCherry (mChe) versions of our control and FUS cells. Synthetic, hypomethylation-
279 mimicking variants which have increased numbers of arginine (i.e., 9R and 16R) were additionally
280 included as further controls (Qamar et al., 2018). We observe that there is a significant impact on the
281 tubular ER network as indicated by a decrease in the ER tubular to sheet ratio compared to the control
282 upon FUS accumulation (**Figure S7A&B**). Furthermore, we also observe a decline in mitochondrial
283 eccentricity (i.e., more rounded structures) in the presence of FUS accumulation, and particularly in
284 P525L-FUS when compared to the control (**Figure S7D&E**), which may indicate defects in mitochondrial
285 fission and increased mitochondrial stress.

286 Since lysosomes also play an important role not only the formation of the ER tubular network
287 but also in protein homeostasis, we analysed their structure and function in the different FUS cells in
288 more detail. To visualise the nanoscale structures of lysosomes in live cells, we again use SIM in mChe(-
289 FUS) COS7 cells (**Figure 4A**, green in Composite). We additionally labelled lysosomes with LysoTracker
290 Deep Red (**Figure 4A,** magenta in Composite), and segmented individual lysosomes from SIM images
291 using a custom-written script (**Figure 4A,** where each lysosome is represented by a different colour). As
292 a positive control, we treated mChe only control cells with chloroquine diphosphate (CQ). As an
293 autophagy inhibitor, CQ promotes the formation and accumulation of autophagosomes, as it disrupts
294 autophagy by preventing lysosome-autophagosome fusion(Mauthe et al., 2018). We observe that
295 R495X (0.28±0.10 μm^2 and 71±12 counted lysosomes) and P525L-FUS (0.29±0.12 μm^2 and 62±9
296 counted lysosomes) have larger and more numerous lysosomes in comparison to WT- (0.12±0.04 μm^2

297 & 46±5 counted lysosomes), 9R- (0.15±0.05 μm^2 & 40±6 counted lysosomes) and 16R-FUS (0.14±0.03
298 μm^2 & 46±7 counted lysosomes), which in turn are larger than in the control (0.09±0.03 μm^2 and 23±3
299 counted lysosomes) (**Figure 4B&C**). As expected, the effect is most prominent in the CQ-added control
300 sample (0.61±0.17 μm^2 and 78±14 counted lysosomes).

301 To test, whether these lysosomes are still able to maintain their low physiological pH, the latter
302 of which is essential to maintain protein homeostasis, we employ Dextran 10,000 MW tagged to Oregon
303 Green 488 (Dex-OG488), which has been used as a pH sensor in a fluorescence lifetime-based assay
304 (Burdikova et al., 2015). Dex-OG488 accumulates in acidic compartments including lysosomes within
305 cells (**Figure 4D**, Composite), hence can be used as an *in situ,* non-invasive lysosomal pH sensor. We
306 measured Dex-OG488 fluorescence lifetime ($\tau_{Dex\text{-}OG488}$) using FLIM and analysed resulting data using fit-
307 free phasor plot analysis. We see modest increases in $\tau_{Dex\text{-}OG488}$ for the nuclear-localised FUS variants,
308 i.e., 3.92±0.99%, 3.67±0.95% (9R) and 4.31±0.72% (16R), in comparison to control cells, which indicates
309 a rise in lysosomal pH. The differences become more significant for the NLS-mutants, i.e., 9.61±0.84%
310 (R495X) and 9.66±0.67% (P525L), as well as CQ-treated control and P525L-FUS (48.4±2.4% and
311 52.4±1.44%, respectively) (**Figure 4E&F**). This is unsurprising as CQ is known to accumulate within
312 lysosomes as a deprotonated weak base, and thereby increases lysosomal pH (Chen et al., 2011). In
313 summary, we see that the dilated lysosomes in ALS-associated P525L- and R495X-FUS have lost their
314 functionality due to greater lysosomal de-acidification.

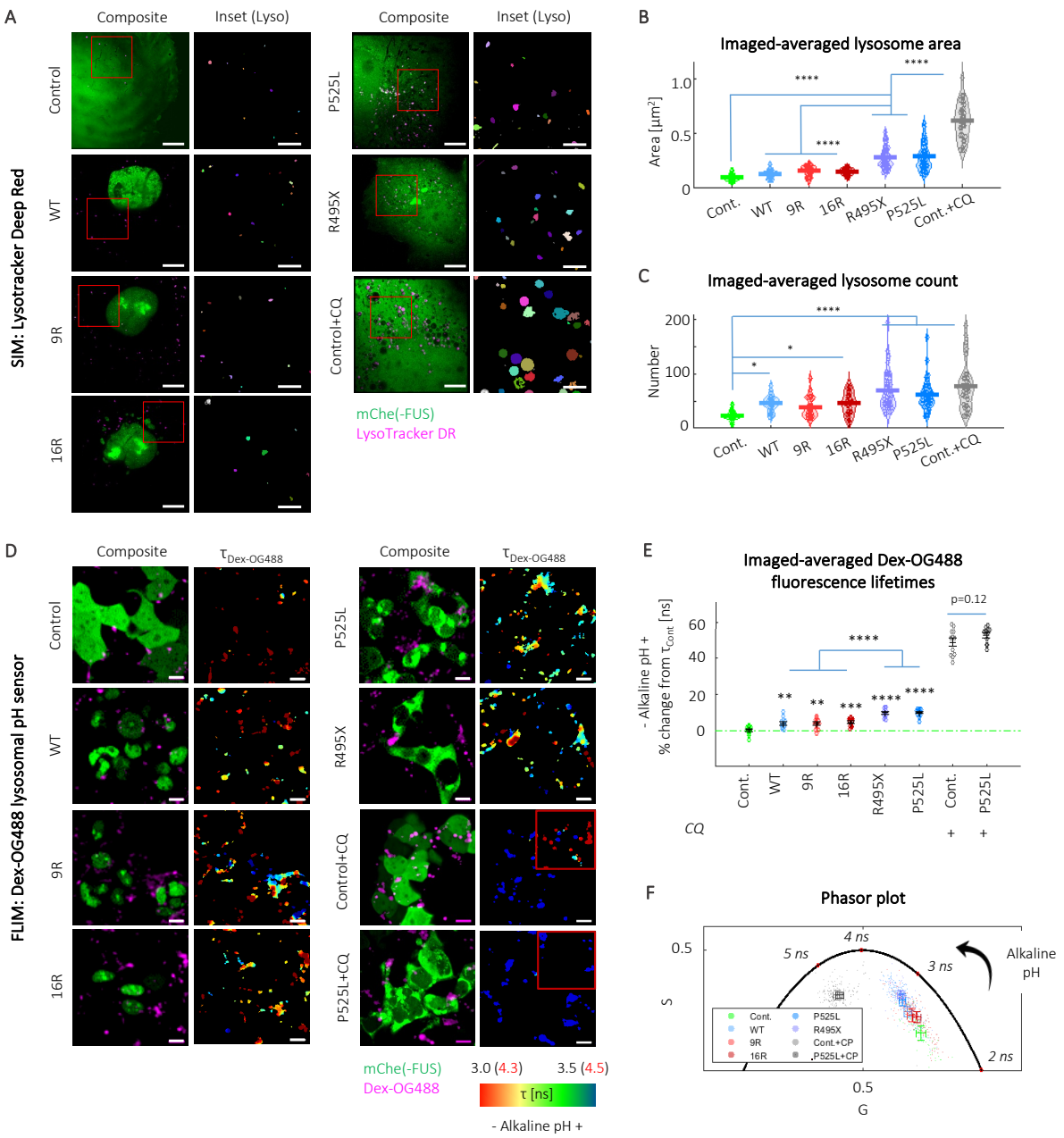

Figure 4: ALS-associated FUS mutants increase lysosomal size and biogenesis, and impact lysosomal pH. (A—C) SIM measurements to visualise lysosomal structure using LysoTracker Deep Red staining. (A) Composite SIM images showing mChe(-FUS) in green and LysoTracker Deep Red in magenta (first column, Composite). Inset corresponds to region within the red box in the Composite image, where individually segmented lysosomes are represented by a different colour. Scale bar, 10 µm. (B) Averaged lysosome area and (C) averaged lysosome count, which show that NLS-mutants, P525L and R495X have more, and Control+CQ has significantly more dilated lysosomes, in comparison to the control and nuclear-localised FUS variants. (D—F) FLIM measurements on Dex-OG488 lysosomal pH sensor. (D) Composite fluorescence intensity images showing mChe(-FUS) in green and Dex-OG488 in magenta (first column, Composite). The latter is used as a non-invasive lysosomal pH sensor with fluorescence lifetime-based readouts shown as falsely coloured images (second column, $\tau_{Dex\text{-}OG488}$).

325 Scale bar, 10 µm. (E) Fit-free phasor plot showing fluorescence lifetime measurements for cell samples, where anti-clockwise
326 direction indicates higher fluorescence lifetime and more alkaline pH. (F) Quantification of fluorescence lifetimes. Analysis is
327 based on 12 images over three biological repeats. Analysis is based on 30—57 cells over three biological repeats. One-way
328 ANOVA (with Holm-Sidak's multiple comparison test), where n.s. is not significant, ** is $p<0.005$, *** is $p<0.001$ and **** is
329 $p<0.0001$.

330 The presence of aberrant FUS aggregation promotes the nuclear translocation of TFEB 331 but not autophagy

332 We have observed that greater lysosomal de-acidification leads to increased lysosomal biogenesis, both
333 of which are enhanced in mutant P525L- and R495X-FUS. De-acidification of lysosomes may trigger
334 autophagy via the nuclear translocation of TFEB, which is a transcriptional modulator for the
335 autophagy-lysosomal pathway (ALP). The latter has been identified as a therapeutic target for diseases
336 involving lysosomal dysfunction (Tan et al., 2021; Willett et al., 2017). Under physiological conditions,
337 TFEB is phosphorylated and remains in the cytoplasm. Nuclear translocation and activation of the TFEB
338 pathway are usually triggered under conditions of starvation and lysosomal stress, leading to
339 autophagosome formation, and increased lysosomal biogenesis that upregulates autophagy
340 (Settembre et al., 2011). Highly expressed in the central nervous system, the dysfunction of TFEB has
341 been implicated in the pathogenesis of numerous neurodegenerative diseases including ALS/FTD (Chen
342 et al., 2015). We thus addressed the role of the TFEB when it translocates from the cytoplasm to the
343 nucleus. Upon co-transfection with GFP-TFEB into mChe(-FUS) HEK293T cells, we observe that there is
344 greater nuclear translocation of TFEB when FUS is co-expressed, which in turn is amplified in the NLS-
345 FUS mutants, P525L and R495X (**Figure 5A&B**). We quantify this as the ratio of nuclear to cytoplasmic
346 fluorescence of GFP-TFEB from widefield images (**Figure 5C**, I_{Nuc}/I_{Cyto}), and validate that the observed
347 effect is predominantly due to FUS expression, as all FUS-expressing cells have I_{Nuc}/I_{Cyto} (e.g., 1.3±0.23
348 to 1.73±0.27 for WT- and P525L-FUS, respectively) that are significantly increased compared to the
349 control cells (0.79±0.17). Control cells were also treated with CQ, which is a known stressor for
350 lysosomal dysfunction, hence result in the induction of nuclear translocation of TFEB (Roczniak-

351 Ferguson et al., 2012) As expected, Control+CQ gives the greatest I_{Nuc}/I_{Cyto} of 2.35±0.31 with 98% of

352 cells showing nuclear translocation (i.e., I_{Nuc}/I_{Cyto} >1); the latter is similar to both R495X and P525L at

353 86% and 90%, respectively.

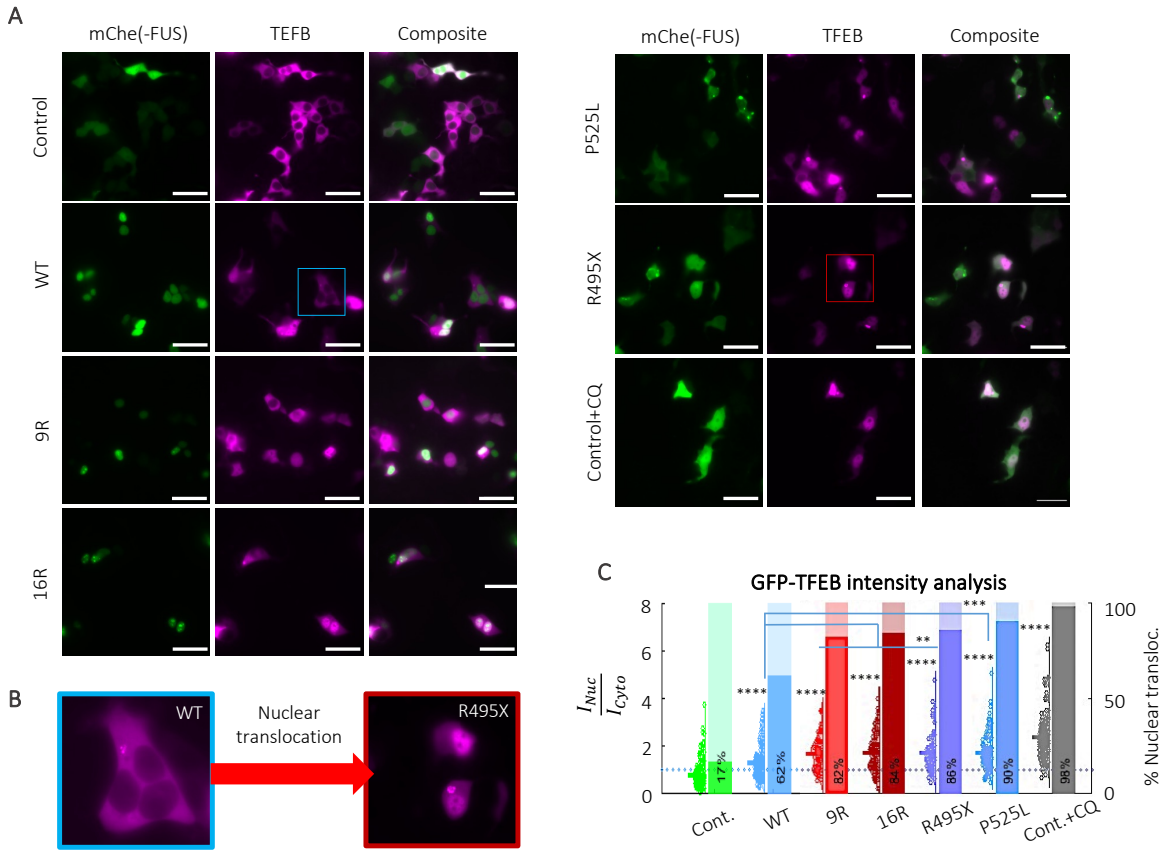

354

355 **Figure 5: Nuclear translocation of TFEB is promoted by FUS accumulation, and in particular for ALS-associated mutants.** (A)

356 Widefield fluorescence intensity images showing mChe(-FUS) in green, GFP-TFEB in magenta and their composite image for

357 all samples tested. Scale bar, 10 µm. (B) Images showing cytoplasmic TFEB expression in WT-FUS, and nuclear translocation in

358 ALS-associated R495X-FUS. (C) Quantification of nuclear to cytoplasmic GFP-TFEB intensities (violin plot, primary y-axis), and

359 their corresponding value of nuclear translocation (bar chart, secondary y-axis), based on images in (A). Mean and S.E.M.

360 values of I_{Nuc}/I_{Cyto}: 0.79±0.17 (Control), 1.31±0.23 (WT), 1.68±0.23 (9R), 1.72±0.26 (16R), 1.70±0.23 (R495X), 1.73±0.27

361 (P525L) and 2.35± 0.31(Control+CQ). Analysis is based on 62—200 cells over three biological repeats. One-way ANOVA (with

362 Holm-Sidak's multiple comparison test), where n.s. is not significant, ** is p<0.005, *** is p<0.001 and **** is p<0.0001.

363

364 We have shown that the presence of FUS accumulation in cells could act as a stressor leading
365 to a loss in acidification of lysosomes, the latter of which trigger the cytoplasmic to nuclear translocation
366 of TFEB, as indicated by the increase in lysosomal biogenesis observed. To address if autophagy is
367 initiated beyond lysosomal biogenesis, we performed Western Blot analysis for autophagy markers, i.e.,
368 p62 and LC3 (**Figure S8A&B**). With FUS accumulation, we observe a slight upregulation of p62, but not
369 of LC3-II, both of which indicate that autophagy is inhibited at this early stage. The most significant
370 difference occurs upon addition of CQ to the control, which drives up normalised LC3-II and p62 by 2-
371 and 5-fold, respectively (**Figure S8B**). Furthermore, a FLIM-based aggregation assay was performed on
372 both GFP-labelled control and P525L-FUS cells, treated with CQ, and rapamycin (i.e., an autophagy
373 inducer). Of the latter, a relatively low concentration of 20 nM introduced in serum-starved media was
374 used, as higher concentrations led to cell death. Fluorescence lifetime of the GFP tag remains the same
375 for P525L-FUS, indicating that there are no changes in the aggregation state of FUS within the cells
376 (**Figure S8C&D**). We thus show that autophagy, and therefore the clearance and degradation of FUS
377 (and other proteins) are inhibited, despite activation of the TFEB-lysosomal pathway. Moreover, at this
378 stage, rapamycin is either toxic to cells at higher doses or not efficacious in reducing FUS aggregation
379 at lower concentrations.

380 # Discussion

381 The experimental data described here reveal that intracellular FUS accumulation leads to i) cytoskeletal
382 and organelle dysfunction and ii) perturbations in cellular homeostasis. To study the latter, we not only
383 analysed different cellular FUS and stress-related models with unprecedented detail but also developed
384 an approach with which we could determine the level of viscosity in live cells.

385 From a micro-rheological standpoint, the liquid condensed state of FUS is a viscoelastic Maxwell
386 fluid, possessing both viscous liquid and elastic solid behaviour (Jawerth et al., 2020). As part of this
387 study, we have developed an approach, based on correlative SPT and FLIM to measure intracellular FUS
388 viscosity. This provides a higher throughput method than FRAP, commonly used in this field, as several
389 condensates can be imaged simultaneously. Moreover, this approach allows us to probe condensates
390 which are smaller than those suitable for more conventional FRAP analysis. It provides a robust route
391 to quantifying this intracellular viscosity, for which there is no existing tool that is widely applicable in
392 the field. We find that NLS-mutants of FUS, P525L- and R495X-FUS, contain more viscous aggregates in
393 comparison to WT-FUS cells. Of the two FUS mutant variants studied, P525L-FUS has the greater
394 aggregation propensity, leading to higher accumulation of drug-induced intranuclear aggregates and
395 SGs. We further show that these mutant variants are also associated with a loss in cytoskeletal
396 mechanoproperties in the cytoplasm, as seen by significant impairment of their actin and tubulin
397 networks. As part of our study, we used SiR-dyes which permit this effect to be captured in live cells, as
398 current studies typically rely on immunofluorescence staining of fixed samples. We further
399 corroborated this using non-fluorescence-based, physical FD-AFM measurements, which show that
400 P525L has half the apparent Young's modulus value of WT-FUS. Similar observations in neuronal models
401 have linked axonal cytoskeletal integrity to the proteinopathy of FUS (Castellanos-Montiel et al., 2020;
402 Giampetruzzi et al., 2019; Theunissen et al., 2021) and other FTD/ALS-implicated proteins, e.g., TAR
403 DNA-binding protein (TDP43) (Baskaran et al., 2018; Briese et al., 2020). This includes a related study in
404 *Xenopus laevis* retinal ganglion cells that demonstrated P525L-FUS reduces actin density specifically in

405 growth cones, resulting in localised softening of the axon(van Tartwijk et al., 2022). Furthermore,
406 several ALS-linked genes that directly impair cytoskeletal dynamics (Castellanos-Montiel et al., 2020;
407 Garone et al., 2020). We further observe that NLS-FUS mutant cells undergo DNA decondensation. At
408 physiological conditions, nuclear-localised FUS regulates DNA repair through its interactions with
409 HDAC1, which becomes dramatically reduced in the case of mutant FUS (Naumann et al., 2018; Wang
410 et al., 2013; Yang et al., 2014) and can in turn increase euchromatin formation (Dinant et al., 2008;
411 Lukas et al., 2011; Miller et al., 2010). Since epigenetic and chromatin regulatory factors are also phase
412 separating in the nucleus (Gibson et al., 2019; Larson et al., 2017; Sanulli et al., 2019; Strom et al., 2017),
413 it is conceivable that mutant, and thus more viscous FUS in the nucleus may also affect epigenetic and
414 chromatin regulatory factors and thereby further enhance euchromatin formation.

415 We, among others, have recently shown that the dysfunction of common biochemical
416 pathways which attenuate organelle function (e.g., lysosomes, ER, mitochondria), are prevalent to
417 multiple neurodegenerative disease(Fowler et al., 2019; Koh et al., 2019; Lu et al., 2020). In
418 combination, they lead to a loss in cellular integrity, and eventually culminate in neuronal dysfunction.
419 To address organelle distribution and function in various cellular FUS and stress-induced models, we
420 applied several different imaging techniques and assays. With ALS-associated mutant P525L-FUS, we
421 observe that increased lysosomal biogenesis leads to lysosomal clustering, as well as mitochondria
422 clustering, at the perinuclear region of cells. As a result, we see a decline in tubular ER due to the loss
423 in lysosomal distribution throughout the cell cytoplasm. Tubular ER is predominantly found in axons,
424 where it modulates synaptic calcium for neurotransmitter release (de Juan-Sanz et al., 2017), and
425 supplies membranes and proteins for synaptic function(Gómez-Suaga et al., 2019). Hence any
426 disruption to its function may have significant consequences for neurons. Additionally, the tubular ER
427 also regulates mitochondrial fission (Merkwirth and Langer, 2008), and thus the mitochondria
428 clustering seen in FUS-expressing cells may influence the latter. P525L-FUS has the largest effect on
429 mitochondria shape, as indicated by the significant loss of eccentricity, i.e., the mitochondria become
430 more circular from a tubular structure, which may stem from the effect of FUS on mitochondrial fission.

431 Many of the above results point towards a dysregulation of the ALP which is supported by
432 previous studies showing aberrant FUS aggregation disrupts the latter (Baskoylu et al., 2022; Soo et al.,
433 2015). We observe cytoplasmic to nuclear translocation of TFEB in the presence of FUS accumulation,
434 which we relate to the higher intralysosomal pH measured in FUS cells. In association, we observe
435 increased lysosomal biogenesis in the absence of changes to autophagy levels. These results support
436 the key role TFEB plays in autophagy regulation, and hence the adverse effects its dysfunction yields.
437 Despite using non-neuronal HEK293T and COS7 cells, we believe the underlying mechanisms observed
438 should hold true for a more physiologically relevant model. In support of this, it was recently shown
439 that there is impaired autophagy and neuronal dysfunction in a P525L-FUS knock in *C. elegans* model
440 (Baskoylu et al., 2022). Moreover, our findings align with the fact that autophagy dysfunction occurs
441 early on in disease pathology, which acts as an accelerator for neurodegeneration (Cortes and la Spada,
442 2019). Autophagy becomes even more vital in the case of aged, i.e., non-/slow-dividing neurones. It has
443 been shown that autophagy-deficient mice are more likely to accumulate aggregation-prone proteins,
444 increasing the risk of neurodegeneration (Hara et al., 2006; Komatsu et al., 2006). Proper function of
445 TFEB and lysosomes have been associated with ageing and longevity (Chang et al., 2017; Lapierre et al.,
446 2015). A recent study has shown that promotion of lysosomal function through the overexpression of
447 Pep4 (i.e., Cathepsin D homologue) in a yeast cell model leads to extended lifespans (Carmona-
448 Gutiérrez et al., 2011). Interestingly, our and the above findings contrast with the interactions of TDP43
449 and TFEB, where it has been shown that the nuclear translocation of TFEB occurs with a deficiency in
450 the first and leads to increased lysosome/autophagosome biogenesis (Xia et al., 2016). However, the
451 loss in TDP43 also leads to downstream impairment of lysosome-autophagosome fusion, leading to an
452 accumulation of autophagic vesicles, and thus both TDP43 and FUS models display autophagy
453 dysfunction. Further studies will be required to pinpoint the exact mechanisms of TFEB-lysosomal
454 dysfunction as well as its impact on organelles, in the presence of aberrant FUS aggregation.
455 Interestingly, many of the defects we have observed as part of our study pinpoint towards an induction
456 of early senescence, such as loss of cellular mechanoproperties, increased euchromatin formation, and

457 loss of protein homeostasis. Aberrant phase transition of FUS had been hypothesised to drive cellular
458 ageing by others in the field (Alberti and Hyman, 2016). It thus remains to be determined whether
459 neuronal cells indeed undergo early senescence as part of a cellular stress induced by aberrant FUS and
460 whether the latter precedes the formation of FUS condensates.

461 There is no current therapeutic strategy for ALS/FTD and many other neurodegenerative
462 diseases. Autophagy inducers, e.g., rapamycin, have been proposed as treatments to alleviate aberrant
463 FUS aggregation (Zhang et al., 2011). However, in our cell models, we did not observe any alleviation in
464 FUS aggregation upon rapamycin treatment. We have previously proposed that perinuclear lysosomal
465 clustering leading to the collapse of the ER network could be a hallmark mechanism across
466 neurodegenerative disease (Lu et al., 2020). Moreover, this has a further impact on cellular integrity
467 and function. For FUS, this is additionally seen in the depolymerisation of cytoskeletal proteins. Hence,
468 potential therapeutic strategies may want to be targeted towards alleviating cytoskeletal defects,
469 organelle dysfunction and perturbations in cellular homeostasis, rather than solely towards aberrant
470 protein aggregation.

471 Our study paints a picture of the effect of aberrant FUS condensates which is highly complex,
472 and impacts many key cellular structures/functions, such as the cytoskeleton, organelles, and cellular
473 homeostasis, which in turn, cannot be alleviated by targeting only one of these defects. Interestingly,
474 many of the above defects mimic signs of early senescence. Indeed, similar features resembling cellular
475 senescence have also been described in other neurodegenerative (Martínez-Cué and Rueda, 2020;
476 Sahu et al., 2022). It remains to be determined whether aberrant proteins first trigger a stress response
477 that affects major cellular functions, such as related to cellular senescence, before or after the
478 formation of aberrant condensates/aggregates. Understanding the latter, will have a major impact on
479 the understanding common factors underlying neurodegenerative diseases and for the development
480 of new therapeutic approaches.

481 # Acknowledgements

482 CWC is funded by the Cambridge Trust and Wolfson College for her PhD. GSKS acknowledges funding
483 from the Wellcome Trust (065807/Z/01/Z) (203249/Z/16/Z), the UK Medical Research Council (MRC)
484 (MR/K02292X/1), Alzheimer Research UK (ARUK) (ARUK-PG013-14), Michael J Fox Foundation (16238)
485 and Infinitus China Ltd. PHStG-H acknowledges funding from the Canadian Institutes of Health
486 Research (406915 Foundation Grant and Canadian Consortium on Neurodegeneration in Aging Grant),
487 Wellcome Trust Collaborative Award (203249/Z/16/Z), US Alzheimer Society Zenith Grant (ZEN-18-
488 529769), Alzheimer Society of Ontario Chair in Alzheimer's Disease Research and National Institute of
489 Aging (U01AG072572; R01AG070864).

490 # Contributions

491 Study conceptualisation and design: GSKS; Cell culture and plasmids: CWC, ADS & AM; Data collection:
492 CWC, AJZ & IM; Data analysis: CWC & AJZ; Feedback: PHStG-H, CFK & TJPK; Draft manuscript
493 preparation: CWC & GSKS; Manuscript editing: all authors. All authors have given approval of the final
494 manuscript.

495 # Declaration of interests

496 The authors declare no competing interests.

497 # Supporting information

498 Methodology and supplementary figures (PDF)

499 # Data availability

500 Raw data is available through Cambridge University Repository Apollo (DOI: 10.17863/CAM.83295).
501 Analysis scripts are available upon request.

References

Alberti S, Hyman AA. 2016. Are aberrant phase transitions a driver of cellular aging? *BioEssays* **38**:959–968. doi:10.1002/BIES.201600042

Aman Y, Schmauck-Medina T, Hansen M, Morimoto RI, Simon AK, Bjedov I, Palikaras K, Simonsen A, Johansen T, Tavernarakis N, Rubinsztein DC, Partridge L, Kroemer G, Labbadia J, Fang EF. 2021. Autophagy in healthy aging and disease. *Nat Aging* **1**:634–650. doi:10.1038/s43587-021-00098-4

Baron DM, Kaushansky LJ, Ward CL, Sama RRK, Chian R-J, Boggio KJ, Quaresma AJC, Nickerson JA, Bosco DA. 2013. Amyotrophic lateral sclerosis-linked FUS/TLS alters stress granule assembly and dynamics. *Mol Neurodegener* **8**:30. doi:10.1186/1750-1326-8-30

Baskaran P, Shaw C, Guthrie S. 2018. TDP-43 causes neurotoxicity and cytoskeletal dysfunction in primary cortical neurons. *PLoS One* **13**. doi:10.1371/JOURNAL.PONE.0196528

Baskoylu SN, Chapkis N, Unsal B, Lins J, Schuch K, Simon J, Correspondence ACH, Hart AC. 2022. Disrupted autophagy and neuronal dysfunction in C. elegans knockin models of FUS amyotrophic lateral sclerosis. *Cell Rep* **38**:110195. doi:10.1016/j.celrep.2021.110195

Bosco DA, Lemay N, Ko HK, Zhou H, Burke C, Kwiatkowski TJ, Sapp P, Mckenna-Yasek D, Brown RH, Hayward LJ. 2010. Mutant FUS proteins that cause amyotrophic lateral sclerosis incorporate into stress granules. *Hum Mol Genet* **19**:4160–4175. doi:10.1093/HMG/DDQ335

Briese M, Saal-Bauernschubert L, Lüningschrör P, Moradi M, Dombert B, Surrey V, Appenzeller S, Deng C, Jablonka S, Sendtner M. 2020. Loss of Tdp-43 disrupts the axonal transcriptome of motoneurons accompanied by impaired axonal translation and mitochondria function. *Acta Neuropathol Commun* **8**:1–16. doi:10.1186/S40478-020-00987-6

Burdikova Z, Svindrych Z, Pala J, Hickey CD, Wilkinson MG, Panek J, Auty MAE, Periasamy A, Sheehan JJ. 2015. Measurement of pH micro-heterogeneity in natural cheese matrices by fluorescence lifetime imaging. *Front Microbiol* **6**:183. doi:10.3389/FMICB.2015.00183

Carmona-Gutiérrez D, Bauer MA, Ring J, Knaue HR, Eisenberg T, Büttner S, Ruckenstuhl C, Reisenbichler A, Magnes C, Rechberger GN, Birner-Gruenberger R, Jungwirth H, Fröhlich KU, Sinner F, Kroemer G, Madeo F. 2011. The propeptide of yeast cathepsin D inhibits programmed necrosis. *Cell Death Dis* **2**:e161. doi:10.1038/CDDIS.2011.43

Castellanos-Montiel MJ, Chaineau M, Durcan TM. 2020. The Neglected Genes of ALS: Cytoskeletal Dynamics Impact Synaptic Degeneration in ALS. *Front Clinic Neurosci* **14**:380. doi:10.3389/FNCEL.2020.594975/BIBTEX

Chang JT, Kumsta C, Hellman AB, Adams LM, Hansen M. 2017. Spatiotemporal regulation of autophagy during Caenorhabditis elegans aging. *Elife* **6**:e18459. doi:10.7554/ELIFE.18459

Chen PM, Gombart ZJ, Chen JW. 2011. Chloroquine treatment of ARPE-19 cells leads to lysosome dilation and intracellular lipid accumulation: Possible implications of lysosomal dysfunction in macular degeneration. *Cell Biosci* **1**:1–10. doi:10.1186/2045-3701-1-10/FIGURES/9

Chen W, Young LJ, Lu M, Zaccone A, Strohl F, Yu N, Schierle GSK, Kaminski CF. 2017. Fluorescence self-quenching from reporter dyes informs on the structural properties of amyloid clusters formed in vitro and in cells. *Nano Lett* **17**:143–149. doi:10.1021/acs.nanolett.6b03686

541 Chen Y, Liu H, Guan Y, Wang Q, Zhou F, Jie L, Ju J, Pu L, Du H, Wang X. 2015. The altered autophagy mediated by
542 TFEB in animal and cell models of amyotrophic lateral sclerosis. *Am J Transl Res* **7**:1574–1587.

543 Conte A, Lattante S, Zollino M, Marangi G, Luigetti M, del Grande A, Servidei S, Trombetta F, Sabatelli M. 2012.
544 P525L FUS mutation is consistently associated with a severe form of juvenile Amyotrophic Lateral
545 Sclerosis. *Neuromuscul Disord* **22**:73–75. doi:10.1016/J.NMD.2011.08.003

546 Cortes CJ, la Spada AR. 2019. TFEB dysregulation as a driver of autophagy dysfunction in neurodegenerative
547 disease: Molecular mechanisms, cellular processes, and emerging therapeutic opportunities. *Neurobiol*
548 *Disease* **122**:83–93. doi:10.1016/J.NBD.2018.05.012

549 Crocker JC, Grier DG. 1996. Methods of Digital Video Microscopy for Colloidal Studies. *J Colloid Interface Sci*
550 **179**:298–310. doi:10.1006/JCIS.1996.0217

551 Davidson NM, Gallimore PJ, Bateman B, Ward AD, Botchway SW, Kalberer M, Kuimova MK, Pope FD. 2020.
552 Measurement of the fluorescence lifetime of GFP in high refractive index levitated droplets using FLIM.
553 *Phys Chem Chem Phys* **22**:14704–14711. doi:10.1039/C9CP06395A

554 de Juan-Sanz J, Holt GT, Schreiter ER, de Juan F, Kim DS, Ryan TA. 2017. Axonal Endoplasmic Reticulum Ca2+
555 Content Controls Release Probability in CNS Nerve Terminals. *Neuron* **93**:867-881.e6.
556 doi:10.1016/j.neuron.2017.01.010

557 Dinant C, Houtsmuller AB, Vermeulen W. 2008. Chromatin structure and DNA damage repair. *Epigenetics*
558 *Chromatin* **1**:9. doi:10.1186/1756-8935-1-9

559 Esbjörner EK, Chan F, Rees E, Erdelyi M, Luheshi LM, Bertoncini CW, Kaminski CF, Dobson CM, Kaminski Schierle
560 GS. 2014. Direct observations of amyloid β Self-assembly in live cells provide insights into differences in
561 the kinetics of Aβ(1-40) and Aβ(1-42) aggregation. *Chem Biol* **21**:732–742.
562 doi:10.1016/j.chembiol.2014.03.014

563 Fowler PC, Garcia-Pardo ME, Simpson JC, O'Sullivan NC. 2019. NeurodegenERation: The Central Role for ER
564 Contacts in Neuronal Function and Axonopathy, Lessons From Hereditary Spastic Paraplegias and Related
565 Diseases. *Front Neurosci* **13**:1051. doi:10.3389/FNINS.2019.01051

566 Fujii S, Takanashi K, Kitajo K, Yamaguchi A. 2016. Treatment with a Global Methyltransferase Inhibitor Induces
567 the Intranuclear Aggregation of ALS-Linked FUS Mutant In Vitro. *Neurochem Res* **41**:826–835.
568 doi:10.1007/s11064-015-1758-z

569 Garone MG, Alfano V, Salvatori B, Braccia C, Peruzzi G, Colantoni A, Bozzoni I, Armirotti A, Rosa A. 2020.
570 Proteomics analysis of FUS mutant human motoneurons reveals altered regulation of cytoskeleton and
571 other ALS-linked proteins via 3'UTR binding. *Sci Rep* **10**:1–8. doi:10.1038/s41598-020-68794-6

572 Giampetruzzi A, Danielson EW, Gumina V, Jeon M, Boopathy S, Brown RH, Ratti A, Landers JE, Fallini C. 2019.
573 Modulation of actin polymerization affects nucleocytoplasmic transport in multiple forms of amyotrophic
574 lateral sclerosis. *Nat Commun* **10**:1–15. doi:10.1038/s41467-019-11837-y

575 Gibson BA, Doolittle LK, Schneider MWG, Jensen LE, Gamarra N, Henry L, Gerlich DW, Redding S, Rosen MK.
576 2019. Organization of Chromatin by Intrinsic and Regulated Phase Separation. *Cell* **179**:484.
577 doi:10.1016/J.CELL.2019.08.037

578 Gómez-Suaga P, Pérez-Nievas BG, Glennon EB, Lau DHW, Paillusson S, Mórotz GM, Calì T, Pizzo P, Noble W,
579 Miller CCJ. 2019. The VAPB-PTPIP51 endoplasmic reticulum-mitochondria tethering proteins are present

580 in neuronal synapses and regulate synaptic activity. *Acta Neuropathol Commun* **7**:35. doi:10.1186/s40478-
581 019-0688-4

582 Gonzalez A, Mannen T, Çağatay T, Fujiwara A, Matsumura H, Niesman AB, Brautigam CA, Chook YM, Yoshizawa
583 T. 2021. Mechanism of karyopherin-β2 binding and nuclear import of ALS variants FUS(P525L) and
584 FUS(R495X). *Sci Rep* **11**:3754. doi:10.1038/s41598-021-83196-y

585 Hara T, Nakamura K, Matsui M, Yamamoto A, Nakahara Y, Suzuki-Migishima R, Yokoyama M, Mishima K, Saito I,
586 Okano H, Mizushima N. 2006. Suppression of basal autophagy in neural cells causes neurodegenerative
587 disease in mice. *Nature* **441**:885–889. doi:10.1038/nature04724

588 Hockings C, Poudel C, Feeney KA, Novo CL, Hamouda MS, Mela I, Fernandez-Antoran D, Vallejo-Ramirez PP,
589 Rugg-Gunn PJ, Chalut K, Kaminski CF, Kaminski-Schierle G. 2020. Illuminating chromatin compaction in live
590 cells and fixed tissues using SiR-DNA fluorescence lifetime. *bioRxiv* 2020.05.02.073536.
591 doi:10.1101/2020.05.02.073536

592 Hofweber M, Hutten S, Bourgeois B, Niessing D, Madl T, Dormann Correspondence D. 2018. Phase Separation of
593 FUS Is Suppressed by Its Nuclear Import Receptor and Arginine Methylation. *Cell* **173**:706-713.e13.
594 doi:10.1016/j.cell.2018.03.004

595 Jawerth L, Fischer-Friedrich E, Saha Suropriya, Wang J, Franzmann T, Zhang X, Sachweh J, Ruer M, Ijavi M, Saha
596 Shambaditya, Mahamid J, Hyman AA, Jülicher F. 2020. Protein condensates as aging Maxwell fluids.
597 *Science (1979)* **370**:1317–1323. doi:10.1126/science.aaw4951

598 Koh JY, Kim HN, Hwang JJ, Kim YH, Park SE. 2019. Lysosomal dysfunction in proteinopathic neurodegenerative
599 disorders: possible therapeutic roles of cAMP and zinc. *Mol Brain* **12**. doi:10.1186/S13041-019-0439-2

600 Komatsu M, Waguri S, Chiba T, Murata S, Iwata JI, Tanida I, Ueno T, Koike M, Uchiyama Y, Kominami E, Tanaka K.
601 2006. Loss of autophagy in the central nervous system causes neurodegeneration in mice. *Nature*
602 **441**:880–884. doi:10.1038/nature04723

603 Kuimova MK. 2012. Mapping viscosity in cells using molecular rotors. *Phys Chem Chem Phys* **14**:12671–12686.
604 doi:10.1039/C2CP41674C

605 Lapierre LR, Kumsta C, Sandri M, Ballabio A, Hansen M. 2015. Transcriptional and epigenetic regulation of
606 autophagy in aging. *Autophagy* **11**:867–880. doi:10.1080/15548627.2015.1034410

607 Larson AG, Elnatan D, Keenen MM, Trnka MJ, Johnston JB, Burlingame AL, Agard DA, Redding S, Narlikar GJ.
608 2017. Liquid droplet formation by HP1α suggests a role for phase separation in heterochromatin. *Nature*
609 **547**:236–240. doi:10.1038/nature22822

610 Lu M, Christensen CN, Weber JM, Konno T, Läubli NF, Scherer KM, Avezov E, Lio P, Lapkin AA, Schierle GSK,
611 Kaminski CF. 2022. ERnet: a tool for the semantic segmentation and quantitative analysis of endoplasmic
612 reticulum topology for video-rate super-resolution imaging. *bioRxiv* 2022.05.17.492189.
613 doi:10.1101/2022.05.17.492189

614 Lu M, van Tartwijk FW, Lin JQ, Nijenhuis W, Parutto P, Fantham M, Christensen CN, Avezov E, Holt CE,
615 Tunnacliffe A, Holcman D, Kapitein L, Kaminski Schierle GS, Kaminski CF. 2020. The structure and global
616 distribution of the endoplasmic reticulum network are actively regulated by lysosomes. *Sci Adv* **6**:7209–
617 7225. doi:10.1126/SCIADV.ABC7209

618 Lukas J, Lukas C, Bartek J. 2011. More than just a focus: The chromatin response to DNA damage and its role in
619 genome integrity maintenance. *Nat Cell Biol* **13**:1161–1169. doi:10.1038/NCB2344

620 Lukinavičius G, Reymond L, D'Este E, Masharina A, Göttfert F, Ta H, Güther A, Fournier M, Rizzo S, Waldmann H,
621 Blaukopf C, Sommer C, Gerlich DW, Arndt HD, Hell SW, Johnsson K. 2014. Fluorogenic probes for live-cell
622 imaging of the cytoskeleton. *Nat Meth* **11**:731–733. doi:10.1038/nmeth.2972

623 Ma Y, Wen K, Liu M, Zheng J, Chu K, Smith ZJ, Liu L, Gao P. 2021. Recent advances in structured illumination
624 microscopy. *J Phys Photonics* **3**:24009. doi:10.1088/2515-7647/abdb04

625 Martínez-Cué C, Rueda N. 2020. Cellular senescence in neurodegenerative diseases. *Front Cell Neurosci* **14**:16.
626 doi:10.3389/FNCEL.2020.00016/BIBTEX

627 Martini-Stoica H, Xu Y, Ballabio A, Zheng H. 2016. The Autophagy–Lysosomal Pathway in Neurodegeneration: A
628 TFEB Perspective. *Trends Neurosci* **39**:221–234. doi:10.1016/J.TINS.2016.02.002

629 Mattenberger Y, James DI, Martinou JC. 2003. Fusion of mitochondria in mammalian cells is dependent on the
630 mitochondrial inner membrane potential and independent of microtubules or actin. *FEBS Lett* **538**:53–59.
631 doi:10.1016/S0014-5793(03)00124-8

632 Mauthe M, Orhon I, Rocchi C, Zhou X, Luhr M, Hijlkema KJ, Coppes RP, Engedal N, Mari M, Reggiori F. 2018.
633 Chloroquine inhibits autophagic flux by decreasing autophagosome-lysosome fusion. *Autophagy* **14**:1435–
634 1455. doi:10.1080/15548627.2018.1474314

635 Merkwirth C, Langer T. 2008. Mitofusin 2 Builds a Bridge between ER and Mitochondria. *Cell* **135**:1165–1167.
636 doi:10.1016/j.cell.2008.12.005

637 Miller KM, Tjeertes J v., Coates J, Legube G, Polo SE, Britton S, Jackson SP. 2010. Human HDAC1 and HDAC2
638 function in the DNA-damage response to promote DNA nonhomologous end-joining. *Nat Struc Mol Biol*
639 **17**:1144–1151. doi:10.1038/NSMB.1899

640 Moreira JMA, Scheipers P, Sørensen P. 2003. The histone deacetylase inhibitor Trichostatin A modulates CD4+ T
641 cell responses. *BMC Cancer* **3**:1–18. doi:10.1186/1471-2407-3-30/FIGURES/7

642 Murakami T, Qamar S, Lin JQ, Schierle GSK, Rees E, Miyashita A, Costa AR, Dodd RB, Chan FTS, Michel CH,
643 Kronenberg-Versteeg D, Li Y, Yang SP, Wakutani Y, Meadows W, Ferry RR, Dong L, Tartaglia GG, Favrin G,
644 Lin WL, Dickson DW, Zhen M, Ron D, Schmitt-Ulms G, Fraser PE, Shneider NA, Holt C, Vendruscolo M,
645 Kaminski CF, St George-Hyslop P. 2015. ALS/FTD Mutation-Induced Phase Transition of FUS Liquid
646 Droplets and Reversible Hydrogels into Irreversible Hydrogels Impairs RNP Granule Function. *Neuron*
647 **88**:678–690. doi:10.1016/j.neuron.2015.10.030

648 Naumann M, Pal A, Goswami A, Lojewski X, Japtok J, Vehlow A, Naujock M, Günther R, Jin M, Stanslowsky N,
649 Reinhardt P, Sterneckert J, Frickenhaus M, Pan-Montojo F, Storkebaum E, Poser I, Freischmidt A,
650 Weishaupt JH, Holzmann K, Troost D, Ludolph AC, Boeckers TM, Liebau S, Petri S, Cordes N, Hyman AA,
651 Wegner F, Grill SW, Weis J, Storch A, Hermann A. 2018. Impaired DNA damage response signaling by FUS-
652 NLS mutations leads to neurodegeneration and FUS aggregate formation. *Nat Commun* **9**:1–17.
653 doi:10.1038/s41467-017-02299-1

654 Nixon-Abell J, Obara CJ, Weigel A v., Li D, Legant WR, Xu CS, Pasolli HA, Harvey K, Hess HF, Betzig E, Blackstone
655 C, Lippincott-Schwartz J. 2016. Increased spatiotemporal resolution reveals highly dynamic dense tubular
656 matrices in the peripheral ER. *Science (1979)* **354**. doi:10.1126/SCIENCE.AAF3928

657 Novo CL, Wong E v., Hockings C, Poudel C, Sheekey E, Wiese M, Okkenhaug H, Boulton SJ, Basu S, Walker S,
658 Kaminski Schierle GS, Narlikar GJ, Rugg-Gunn PJ. 2022. Satellite repeat transcripts modulate
659 heterochromatin condensates and safeguard chromosome stability in mouse embryonic stem cells. *Nat*
660 *Commun* **13**:1–16. doi:10.1038/s41467-022-31198-3

Pu J, Guardia CM, Keren-Kaplan T, Bonifacino JS. 2016. Mechanisms and functions of lysosome positioning. *J Cell Sci* **129**:4329. doi:10.1242/JCS.196287

Qamar S, Wang GZ, Randle SJ, Ruggeri FS, Varela JA, Lin JQ, Phillips EC, Miyashita A, Williams D, Ströhl F, Meadows W, Ferry R, Dardov VJ, Tartaglia GG, Farrer LA, Kaminski Schierle GS, Kaminski CF, Holt CE, Fraser PE, Schmitt-Ulms G, Klenerman D, Knowles T, Vendruscolo M, St George-Hyslop P. 2018. FUS Phase Separation Is Modulated by a Molecular Chaperone and Methylation of Arginine Cation-π Interactions. *Cell* **173**:720-734.e15.

Roczniak-Ferguson A, Petit CS, Froehlich F, Qian S, Ky J, Angarola B, Walther TC, Ferguson SM. 2012. The Transcription Factor TFEB Links mTORC1 Signaling to Transcriptional Control of Lysosome Homeostasis. *Sci Signal* **5**:ra42. doi:10.1126/SCISIGNAL.2002790

Sahu MR, Rani L, Subba R, Mondal AC. 2022. Cellular senescence in the aging brain: A promising target for neurodegenerative diseases. *Mech Ageing Dev* **204**:111675. doi:10.1016/J.MAD.2022.111675

Sama RRK, Ward CL, Kaushansky LJ, Lemay N, Ishigaki S, Urano F, Bosco DA. 2013. FUS/TLS assembles into stress granules and is a prosurvival factor during hyperosmolar stress. *J Cell Physiol* **228**:2222. doi:10.1002/JCP.24395

Sanulli S, Trnka MJ, Dharmarajan V, Tibble RW, Pascal BD, Burlingame AL, Griffin PR, Gross JD, Narlikar GJ. 2019. HP1 reshapes nucleosome core to promote phase separation of heterochromatin. *Nature* **575**:390–394. doi:10.1038/s41586-019-1669-2

Schwerk C, Schulze-Osthoff K. 2005. Methyltransferase inhibition induces p53-dependent apoptosis and a novel form of cell death. *Oncogene* **24**:7002–7011. doi:10.1038/sj.onc.1208855

Settembre C, di Malta C, Polito VA, Arencibia MG, Vetrini F, Erdin S, Erdin SU, Huynh T, Medina D, Colella P, Sardiello M, Rubinsztein DC, Ballabio A. 2011. TFEB links autophagy to lysosomal biogenesis. *Science (1979)* **332**:1429–1433. doi:10.1126/SCIENCE.1204592

Soo KY, Sultana J, King AE, Atkinson R, Warraich ST, Sundaramoorthy V, Blair I, Farg MA, Atkin JD. 2015. ALS-associated mutant FUS inhibits macroautophagy which is restored by overexpression of Rab1. *Cell Death Disc* **1**:15030. doi:10.1038/cddiscovery.2015.30

Strom AR, Emelyanov A v., Mir M, Fyodorov D v., Darzacq X, Karpen GH. 2017. Phase separation drives heterochromatin domain formation. *Nature* **547**:241–245. doi:10.1038/nature22989

Tan A, Prasad R, Jho E hoon. 2021. TFEB regulates pluripotency transcriptional network in mouse embryonic stem cells independent of autophagy–lysosomal biogenesis. *Cell Death Dis* **12**:1–14. doi:10.1038/s41419-021-03632-9

Theunissen F, West PK, Brennan S, Petrović B, Hooshmand K, Akkari PA, Keon M, Guennewig B. 2021. New perspectives on cytoskeletal dysregulation and mitochondrial mislocalization in amyotrophic lateral sclerosis. *Transl Neurodegener* **10**:1–16. doi:10.1186/S40035-021-00272-Z

van Tartwijk FW, Wunderlich LCS, Mela I, Makarchuk S, Jakobs M, Qamar S, Franze K, Kaminski Schierle GS, St George-Hyslop P, Lin JQ, Holt CE, Kaminski CF. 2022. Mutation of the ALS/FTD-associated RNA-binding protein FUS alters axonal cytoskeletal organisation . *bioRxiv*.

Vigushin DM, Ali S, Pace PE, Mirsaidi N, Ito K, Adcock I, Charles Coombes R. 2001. Trichostatin A Is a Histone Deacetylase Inhibitor with Potent Antitumor Activity against Breast Cancer in Vivo 1. *Clin Cancer Res* **7**:971–976.

701 Waibel S, Neumann M, Rabe M, Meyer T, Ludolph AC. 2010. Novel missense and truncating mutations in
702 FUS/TLS in familial ALS. *Neurol* **75**:815–817. doi:10.1212/WNL.0B013E3181F07E26

703 Wang WY, Pan L, Su SC, Quinn EJ, Sasaki M, Jimenez JC, MacKenzie IRA, Huang EJ, Tsai LH. 2013. Interaction of
704 FUS and HDAC1 regulates DNA damage response and repair in neurons. *Nat Neurosci* **16**:1383–1391.
705 doi:10.1038/NN.3514

706 Willett R, Martina JA, Zewe JP, Wills R, Hammond GRV, Puertollano R. 2017. TFEB regulates lysosomal
707 positioning by modulating TMEM55B expression and JIP4 recruitment to lysosomes. *Nat Commun* **8**:1–17.
708 doi:10.1038/s41467-017-01871-z

709 Wolozin B, Ivanov P. 2019. Stress granules and neurodegeneration. *Nat Rev Neurosci* **20**:649–666.
710 doi:10.1038/s41583-019-0222-5

711 Xia Q, Wang H, Hao Z, Fu C, Hu Q, Gao F, Ren H, Chen D, Han J, Ying Z, Wang G. 2016. TDP-43 loss of function
712 increases TFEB activity and blocks autophagosome–lysosome fusion. *EMBO J* **35**:121–142.
713 doi:10.15252/EMBJ.201591998

714 Yang L, Gal J, Chen J, Zhu H. 2014. Self-assembled FUS binds active chromatin and regulates gene transcription.
715 *Proc Natl Acad Sci USA* **111**:17809–17814. doi:10.1073/PNAS.1414004111

716 Yang P, Mathieu C, Kolaitis RM, Zhang P, Messing J, Yurtsever U, Yang Z, Wu J, Li Y, Pan Q, Yu J, Martin EW,
717 Mittag T, Kim HJ, Taylor JP. 2020. G3BP1 Is a Tunable Switch that Triggers Phase Separation to Assemble
718 Stress Granules. *Cell* **181**:325-345.e28. doi:10.1016/J.CELL.2020.03.046

719 Young LJ, Ströhl F, Kaminski CF. 2016. A Guide to Structured Illumination TIRF Microscopy at High Speed with
720 Multiple Colors. *J Vis Exp* **111**:e53988. doi:10.3791/53988

721 Zhang Xiaojie, Li L, Chen S, Yang D, Wang Y, Zhang Xin, Wang Z, Le W. 2011. Rapamycin treatment augments
722 motor neuron degeneration in SOD1G93A mouse model of amyotrophic lateral sclerosis. *Autophagy*
723 **7**:412–425. doi:10.4161/AUTO.7.4.14541

724

725